# Thermal Spike model

Kaling Vikram Singh [1]

**Abstract**
The thermal spike model is an important tool for understanding how materials behave under high energy inputs, such as ion irradiation. This model represents the occurrence of localised, rapid temperature increases within the material, sometimes known as ”thermal spikes”. These spikes are extremely localised, spanning nanometer length scales and picosecond durations, making them difficult to investigate experimentally. As a result, computer models play an important role in understanding these occurrences. The model explains how energy is accumulated and diffused in the lattice, resulting in defects, phase transitions, and even melting. However, the model has drawbacks, such as assuming immediate and localised energy deposition and failing to account for specific quantum mechanical processes. Despite these limitations, the thermal spike model provides unique insights into material behaviour under high temperatures and has important implications for the design and optimisation of materials exposed to ion irradiation. The model is limited by the computational power of the simulation system. In this work, we have irradiated Cu and Ni ions with 700 KeV Xe ions to study the thermal spikes.

**Keywords**
Thermal spike – Explicit Euler – Stopping power

[1] *National Institute of Science Education and Research, Roll 2011074*

## Contents



## Objectives

- To calcualte the thermal spike in ion beam irradiated metal.
- To extend the model to multiple layers.
- To study the evolution of temperature over time and space.

## 1. Introduction

Swift heavy ions (SHIs) produced at major accelerator facilities are capable of producing beams of high mass ions with kinetic energy ranging from MeV to GeV or higher. In many substances, SHIs release enough energy to create long, nanometer-sized damage trails known as ’latent tracks’ or ’ion tracks’ because they are invisible to the naked eye or optical microscopy. These also induce atomic movements leading to defects in materials. SHIs are extensively used in domains like nuclear detection, geochronology, archaeology, and many more. Particularly, in material sciences, these irradiations are used for synthesis of nanostructures such as quantum dots and quantum wells [1, 2].

When materials are irradiated with SHIs, the input energy is primarily transferred to the target’s electrons, with no direct atomic displacement, as is the case with irradiation in nuclear collisions. Two models have been proposed to explain the appearance of latent tracks in matter caused by the slowing of incident ions in the electronic stopping power regime. The first was Desauer’s proposed thermal spike model for insulators in 1923, which was then extended by Seitz and Koehler for metals in 1965 [3]. The second was the ionic spike, proposed by Fleischer et al. [4], which explained why metals are insensitive to the electronic excitation caused by fission fragments. The Coulomb repulsion between ionised lattice atoms in the ionic spike model is proportional to the time spent screening by returning electrons. Ionic Spike Model focuses on the atomic collision cascade induced by the primary ionizations. It describes the disordered zone around the ion trajectory, which is associated with cylindrical damage-regions several nanometers in diameter. On the other hand, Thermal Spike Model is concerned with the secondary electrons induced by a radiation effect in the material. In the thermal spike model, the spread of energy in the electron subsystem is determined by electron mobility. The passage of a fast ion through a material creates a ’heat spike’ along its path, in which the temperature

may be briefly extremely high, even if the average temperature of the material remains low. The thermal spike model explains the way electron mobility affects energy distribution in the electron subsystem. In all instances, high mobility favours reduced efficiency of track creation in metals. The time scales of ionic spike is $10^{-14}$s - $10^{-13}$s while that of the thermal spike model is $10^{-12}$s - $10^{-14}$s. Since the experiments are carried at higher time scales, we resort to thermal spike model for the study of irradiations.

### 1.1 Thermal Spike Model

It is a theoretical framework in Debye model that describes the effects of ion beam irradiation on a material. When ion penetrates a solid, it loses energy through two nearly independent processes: (a) electronic excitation and ionization (i.e. electronic slowing down '$S_e$', or electronic energy loss $S_e$ = (dE/dz)) and (b) collisions with the atomic nuclei ($S_n$). These can be thought of 4 sub-processes: (a) Energy transfer to electrons through ionisation, (b) Energy transfer to cold electrons through collisions, (c) Electron phonon interactions leading to local heating and quenching and finally, (d) dissipations. When ion energy is lost in a solid due to electronic slowness, the electronic system locally experiences rapid heating up to a temperature T, which is on the same order of magnitude as the Fermi temperature. The deposited energy is subsequently shared by the target electrons and the lattice atoms through electron-electron and electron-phonon interactions. When we take into account the electron - phonon coupling, the model is referred to as inelastic thermal spike (i-TS) model. Electronic stopping power ($S_e$) and nuclear stopping power ($S_n$) are defined as the energy losses of the radiation due to interaction with the material.

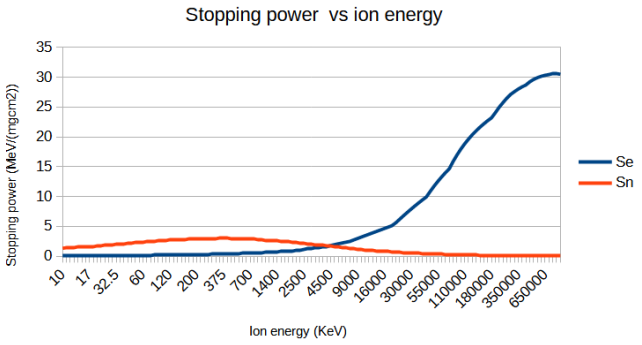


**Figure 1.** $S_e$ vs $S_n$ for Xe irradiation on Au

We have 2 subsystems that are independent, the electronic lattice and the atomic (or nuclear) lattice. At higher energies, heat transfer to electronic lattice is dominant, i.e $S_e >> S_n$, and $S_n$ can be neglected . Assuming that we are in the low energy regime ($\sim$ KeV), the nuclear and electronic stopping powers are comparable and cannot be neglected. SRIM 2010 [5] was used to get the relation between $S_n$ and $S_e$ for different ion energies, as shown in fig 1. Besides this, at low energy irradiations, the $S_n$ and $S_e$ remain nearly constant. For thin

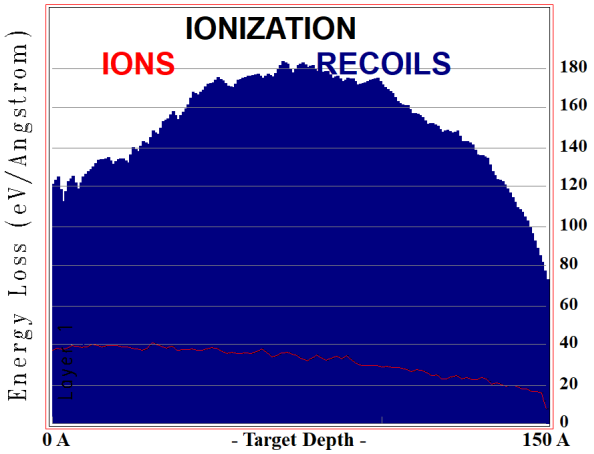


**Figure 2.** $S_e$ and $S_n$ vs depth for Xe irradiation on Au

films, we can assume $S_n$ and $S_e$ to be nearly constant and can be averaged out. This can be seen in fig 2, obtained by SRIM cascade of 2000, 100 KeV Xe irradiations on 15nm long Au sample. The $S_n$ and $S_e$ remain nearly constant for lengths 3 nm - 9 nm . For longer samples, the plot can be used to get $S_n$ and $S_e$ as functions of depth **x**. The dynamics is governed by the heat equation in cylindrical coordinate system and the net heat transfer is given by:

$$\begin{aligned} C_e\frac{\partial T_e}{\partial t} &= \frac{1}{r}\frac{\partial}{\partial r}\left(rK_e(T_e)\frac{\partial T_e}{\partial r}\right)+\left(\frac{\partial}{\partial x}K_e(T_e)\frac{\partial T_e}{\partial x}\right) \\ &\quad -g(T_e-T_a)+A(r,t), \\ C_a\frac{\partial T_a}{\partial t} &= \frac{1}{r}\frac{\partial}{\partial r}\left(rK_a(T_a)\frac{\partial T_a}{\partial r}\right)+\left(\frac{\partial}{\partial x}K_a(T_a)\frac{\partial T_a}{\partial x}\right) \\ &\quad +g(T_e-T_a)+B(r,t), \end{aligned} \tag{1}$$

where, $C_{e,a}$, $T_{e,a}$, and $K_{e,a}$ are the specific heat, temperature, and thermal conductivity of the electronic and atomic subsystems, respectively. g is the electron phonon coupling coefficient and the heat transfer to the is given by the term g($T_e$ - $T_a$). A(r,z,t) and B(r,z,t) are source terms that are dependent on the irradiation and the material properties and are called source energy density terms for electronic and nuclear lattices respectively. The r and x terms corresponds to heat transfer in radial direction and axial directions respectively. In the general case, the function A(r,z,t) is the volume density of power deposited by the ion. It can be represented in the following most commonly used form:

$$A(r,z,t) = b_e S_{e(z)} \exp\left(-\frac{(t-t_0)^2}{2\sigma_t^2}\right)\exp(-r/r_0) \tag{2}$$

The time of electron equilibration (free passing of $\delta$ electrons with an average energy of $\varepsilon_e$ ) is t = (1-5)·10x$^{-15}$ s, with the half-width at full maxima ($\sigma_0$) of the distribution asuumed to be equal to $t_0$. The decay rate or the highly excited spatial width $r_0 \leq$ is between 1 - 2.5 nm [6]. $b_e$ is the normalization

factor given by:

$$\int_0^\infty dt \int_0^{r_m} 2\pi r A(r,z,t)dr = S_e = S_{e0}\mu(z). \quad (3)$$

where, $r_m$ is the maximum path travelled by $\delta$ electrons. For longer samples, $S_e$ is a function of z, and $\mu(z)$ can be used as the fit fuction, calculated from SRIM ionisation data, as shown in fig 2. On integrating 3, and assuming $\frac{r_m}{r_0} >> 1$ and thin samples:

$$b_e \approx \left\{(2\pi)^{3/2} \times 0.84134 r_0^2 t_0\right\}^{-1}. \quad (4)$$

Similarly, B(r,z,t) is considered as the energy density source term for the atomic lattice and given by:

$$B(r,z,t) = \frac{b_n S_n e^{-t/\tau} e^{-r/R_0}}{r} \quad (5)$$

The the exponential decay ($\tau$) can be estimated from the cascade as shown in 2. According to TRIM-SP simulations a few keV are deposited to each atom, resulting in a typical range of 10 Å. From this, we get $\tau$ in the range of $10^{-13}$ - $10^{-13}$s. $R_0$ , called the spike radius (where 66% of the total nuclear energy is deposited), can also be calcualted through the TRIM cascade and is in the order of 15 - 20 Å. It is tough to calculate the value of g, but it is can be estimated for insulators as:

$$g = 2/\lambda \quad (6)$$

where $\lambda$ is the mean free path of the phonons. For defining A and B, we need the relative time scales of the processes and the radius ($r_0$) in which the energy deposition occurs. $r_0$ can be found using peak area for absorption for a given wave number and finding the cross section in which the probability of deposition is high. To determine ro, the mean energy transfer <T> to sample atoms is calculated from the screened elastic scattering cross section [7]. This was then used to obtain ro using the procedure mentioned by Toulemonde et al. [8]. We want thermal spike not to exceed the energy required to induce a phase transition from solid to gas. The energy required to induce such trasnitions ($E_a m$) is given by:

$$E_{am} = \int_{T_0}^{T_{melt}} C_s(T)dT + L_m \quad (7)$$

where $C_s$ is lattice specific heat, $T_0$ is initial temperature, $T_{melt}$ is melting temperature and $L_m$ is the latent heat of fusion. Such transitions lead to molten phases, which leads to defects in the irradiated material. In the current system, we assume that the metals have very high melting point, and we just discuss the temperature variation of the irradiated material.

## 2. Numerical calculations

The physical quantities are made unitless, to reduce dependence on units that may lead to large errors at long iterations. Also to reduce computation times and achieve better accuracies, the following transformations are made:

$$\bar{t} = \frac{t}{\alpha_1 t0}$$
$$\bar{r} = \frac{r}{\alpha_2 r0}$$
$$\bar{z} = \frac{z}{\alpha_2 r0}$$

where $\alpha_1$ = $\alpha_2$ = 100. Further, we introduce a variable in exponential term of A, which reduces the dependence of temperature on time by $e^{12}$, making the system more realistic. Since the thermal conductivity is temeperature dependent at a given point, we use chain rule to obtain:

$$\begin{aligned} C_e(T_e)\frac{\partial T_e}{\partial t} &= K_e(T_e)\left\{\frac{1}{r}\frac{\partial T_e}{\partial r} + \frac{\partial^2 T_e}{\partial r^2} + \frac{\partial^2 T_e}{\partial x^2}\right\} \\ -g(T_e - T_i) + A(r,x,t) &+ \frac{\partial K_e}{\partial T_e}\left(\left(\frac{\partial T_e}{\partial r}\right)^2 + \left(\frac{\partial T_e}{\partial x}\right)^2\right) \end{aligned} \quad (8)$$

$$\begin{aligned} C_a(T_a)\frac{\partial T_a}{\partial t} &= K_a(T_a)\left\{\frac{1}{r}\frac{\partial T_a}{\partial r} + \frac{\partial^2 T_a}{\partial r^2} + \frac{\partial^2 T_a}{\partial x^2}\right\} \\ +g(T_e - T_a) + B(r,x,t) &+ \frac{\partial K_a}{\partial T_a}\left(\left(\frac{\partial T_a}{\partial r}\right)^2 + \left(\frac{\partial T_a}{\partial x}\right)^2\right) \end{aligned}$$

Applyting the transformations, we get:

$$A(r,z,t) = \frac{B_e S_e \alpha 1 t_0}{T_0} e^{-\alpha_2 \cdot r} e^{-\alpha_1^2 \cdot (t-0.05)^2/2} \quad (9)$$

$$B(r,z,t) = \frac{S_n B_n \alpha_1 t_0}{\alpha_2 r_0 T_0} e^{-\alpha_2 r} e^{-\alpha_1 t_0 t/\tau}/r \quad (10)$$

The boundary conditions are given by( bars on variables will be removed for simplicity):

$$\bar{T}_{e/a}(r,z,0) = 1 \quad (11)$$

$$\bar{T}_{e/a}(r,z,t) = 1 \quad (For \;\; r = r_{max} \;\; or \;\; z = z_{max}) \quad (12)$$

$$\frac{\bar{T}_{e/a}(r,z,t)}{\partial(r)} = \frac{\bar{T}x_{e/a}(r,z,t)}{\partial(z)} = 0 \quad (For \;\; r = z = 0) \quad (13)$$

We use explicit schemes to solve these equations. We divide the space and time coordinates of equation into finite number of intervals. Then, we use finite differences to find the dynamics of the heat equation. Let define the finite differences by dr = $\Delta r$,dz = $\Delta z$,dt = $\Delta t$ (Assuming initially, r = z = t = 0): The first order derivative is given by:

$$\frac{\partial T_e(r,z,t)}{\partial r} = \frac{T_e((i+1)\Delta r,z,t) - T_e((i-1)\Delta r,z,t)}{2\Delta r} \quad (14)$$

where i is the iteration step. Similarly, derivatives with z and t are defined. The second order derivative is given by (derivatives with respect to z and t can be defined similarly):

$$\frac{\partial^2 T_e(r,z,t)}{\partial r^2} = \frac{T_e((i+1)\Delta r,z,t) + T_e((i-1)\Delta r,z,t) - 2T_e(i\Delta r,z,t)}{(\Delta r)^2} \tag{15}$$

In the python code, we use arrays of Te, Ta with fixed dimensions and update the temperature parameter by traversing through the spatial coordinates for a given time **n** and iterate over the time parameter untill we reach the dersired time scale. Using 15 and 14, we arrive at the finite difference equation:

$$T_e[i,j,n+1] = T_e + (\frac{K_e \Delta t}{C_e})[\frac{(\frac{\partial T_e}{\partial r})}{i\Delta r} + \frac{\partial^2 T_e}{\partial r^2} + \frac{\partial^2 T_e}{\partial z^2}] - (\frac{\Delta t}{C_e})(g\alpha_1 t0)(T_e - T_a) + \frac{\Delta t}{C_e} A(i,j,n) \tag{16}$$

All the $T_e$ and $T_a$ on RHS are instantaneous electronic and lattice temperatures respectively, i.e $T_\nu$ = $T_\nu$[i,j,n] and $\nu$ = a,b. While doing this, we have assumed that $\frac{\partial K_\nu}{\partial T_\nu} = 0$, i.e specific heat is nearly constant with change of temperature, which can be modified bvy just adding the $\frac{\partial K_\nu}{\partial T_\nu}$ term using the same finite difference process, as other parameters are known. Similarly, we can get:

$$T_a[i,j,n+1] = T_a + (\frac{K_a \Delta t}{C_a})[\frac{(\frac{\partial T_a}{\partial r})}{i\Delta r} + \frac{\partial^2 T_a}{\partial r^2} + \frac{\partial^2 T_a}{\partial z^2}] + (\frac{\Delta t}{C_a})(g\alpha_1 t0)(T_e - T_a) + \frac{\Delta t}{C_a} B(i,j,n) \tag{17}$$

Now, once this was fixed, the values of constants were obtained from Wangts et.al [6, 8, 9]. We chose Cu substrate irradiated with Uranium ion with energy 700 KeV. The $S_e$ and $S_a$ values were obtained from SRIM 2008 and TRIM [10] calculations. Note that the SRIM calculations are based on monte carlo simulations of ion trajectory casades that have reported about a 10% error bar. Thus, our calculations would have atleast an error bar of 10%. The following values were used:

$$\begin{aligned} &C_a = 0.36 + 8.6 * 10^{-5} * T + 2.9 * 10^{-9} * T^2 \\ &\text{if } T_a < 1358/T_0, \text{ else } 0.5 \\ &C_e = 12.682 * T \text{if } T_a < 1795.5/T_0, \text{ else } 227554.754 \\ &K_e = 3.5 * 10^2/(T_e^2) \end{aligned} \tag{18}$$

Note that since we are using an explicit euler method, using partial difference, we encounter a stability issue, thus, we have a condition for the values of $\Delta t$, $\Delta z$ and $\Delta r$, given by:

$$K_e \cdot \Delta t(\Delta r^{-2} + \Delta z^{-2}) \leq 0.5 \tag{19}$$

Values of A, B are calculated from the SRIM calculations and [6] and can be found in the code, at http://surl.li/ssifn.

Next, the job was to make the system for more than one layers. For the thin layer, we assume ideal contacts. Ideal contacts are ones which do not introduce external potentials in the dynamics, such as contact resistances, gaps etc. In such conditions, the rate of gain of heat for subsystem 2 shall be equal to rate of trasnfer of heat from the subsystem 1. Also, since the materials are in contact, they shall not have any gaps, thus, continuity of temperatures is necessary. Thus, we have the following conditions:

$$\begin{aligned} T^1_{e/a}(r,z=h^-,t) &= T^1_{e/a}(r,z=h^+,t) \\ K^1_{e/a}(r,z=h,t)\frac{\partial T^1_{e/a}}{\partial z} &= K^2_{e/a}(r,z=h,t)\frac{\partial T^2_{e/a}}{\partial z} \end{aligned} \tag{20}$$

where h is the position of the contact of the two layers. Using these two equations at the boundary, the above equations 17 and 16, the monolayer system can be expanded to multilayer system. In this work, a monolayer and a bilayer system have been studied under Xe ion irradiations. This was done by using a Ni substrate along with same irradiations, considering the intensities do not change much over space. The loss is given by ($\Delta$ z· ($S_e$ + $S_a$)) $\approx$ 36 KeV. The values do not change drastically over space (thin film approximations). Thus, the irradiation (of Xe ions) to the Ni substate is nearly 660 KeV. Again, we perform SRIM calculations to get the valeus of $S_e$ and $S_a$. The values of $S_e$ and $S_a$ would again have error bars of $\sim$%, thus the results are approximated to have around 15-25 % error rates. Although, it provides a good enough approximation to study the basic dynamics of the irradiated systems [11].

## 3. Observations

### 3.1 Observations for Monolayer thermal spike

For a monolayer system, it was observed that an overall gaussian temeperature distribution in both r and z axis. The boundaries are cooled at 20 K, initial temperature of the system. Various plots to understand the system dynamics were observed:

First, the variation of temperature with spacial parameters shown. It was observed that there is a particular region (2.5 - 3 nm), ref:fig 5 , along axial and (2.5-2.7nm), ref fig:**??**, in the radial direction, where we observed highest spike in temperatures. This is due to effects of the boundaries and the heat transfer from the boundaries lead to lower temperatures near the edges of the sample. The temperature is highest as some distance from the boundaries.

Second, we plotted the evolution of temperatures with changing time at different radii and axial distances. It was observed that the region near the boundary had a cross over time, when the region farther away from the (0,0,0) origin experiences higher temeperatures than the closer region, ref fig:6 and fig:7, in the radius 5 Å, 12.5 Åand axial distances 5 Å, 12.5 Årespectively . This was due to backflow of heat

from these high temperatues region and travelling of the ion beam through the medium that raises the temperatures.
Third, since the stopping power in the eletronic lattice was low, we observed low temperatures in the electronic lattices at low energy irradiance. If the irradiance is increased, we see the temperature of the electronic lattice is much higher than the nuclear lattice.

Finally, there was a region that saturated in temperature and there was no further increase upto timescales of $10^{-14}$s. We could not see the evolution at larger time scales than $10^{-14}$s due to lack of powerful computers. Similar works [12, 13, 6, 14] note that there is decrease in temperature of electronic lattices, but the lattice temperatures saturate and may decrease over time due to heat dissipation. This heat dissipation is maximum near the surfaces, which is visible in fig6, where the temperature decreases when the region of interest is far away from the central beam.

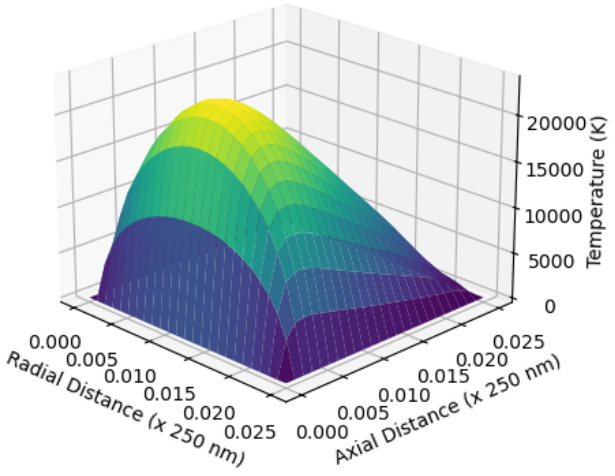


**Figure 3.** Evolution of total temperature with space.

### 3.2 Observations for multilayer thermal spike

The dynamics of the bilayer system is similar to monolayer dynamics inside the second substrate. The interesting change in temperatures were noted near the contact boundary. We also observed a dip in the temperature near the contact. The faster heat transfer to the second substate may lead to this phenomena. The heat may be transferred to back into the first substrate in the peripheri, conpared to being trasnferred copletely. The temperature chage is not visible properly in fig9 as it contains the temperature dynamics in 3D plots. A better view is given in fig 8. It shows that near the contact boundary (6.25nm), we see gradual temperature drops then it increases back. The width of the low temperature can be reduced if we take finer axial distances, but this puts a bound on the time scales we are looking at. Thus, we had to compromise the axial change to see the dynamics at higher time scales. The increase in temeprature in the second substrate (Ni) is due to the fact that it has higher stopping powers, thus more

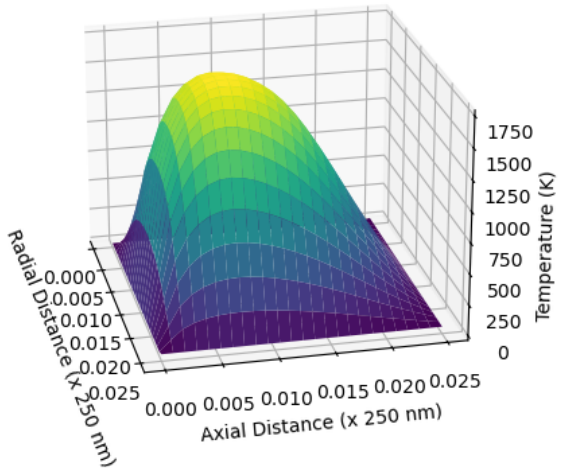


**Figure 4.** Evolution of electronic lattice temperature with space.

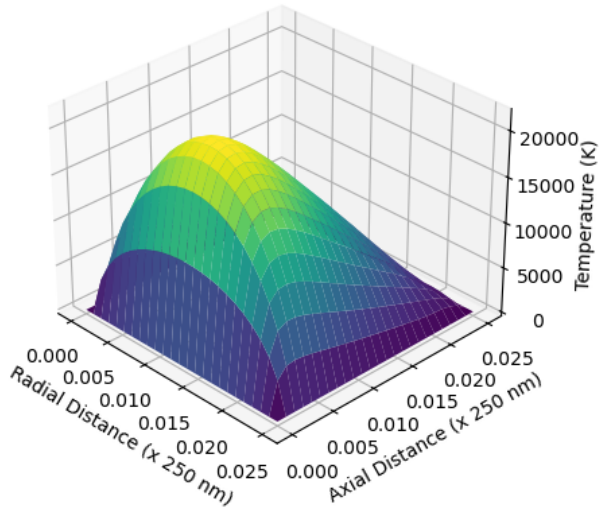


**Figure 5.** Evolution of nuclear lattice temperature with space.

collsions occur and induce more heat into the system. Also, as visible from the fig 9, there is an abrupt increase in the temeperatures after the contact places, which shows that there is a discontinuity near in the derivative of termperatures at the contact surfaces.The plots are different than before as the plots are plotted at lower time scales(to save computational power). These pltos provide an indicative idea about the physics near the contact. The exact physics would be tough to simulate since we need to add non ideal contacts and potentials in order to look incorporate the surface phenomena. The lower time scales were chosen, again due to memory issues (RAM).

## 4. Discussion and conclusion

It was observed that there was a substantial increase in the temperature of the irradiated material over time. Since the

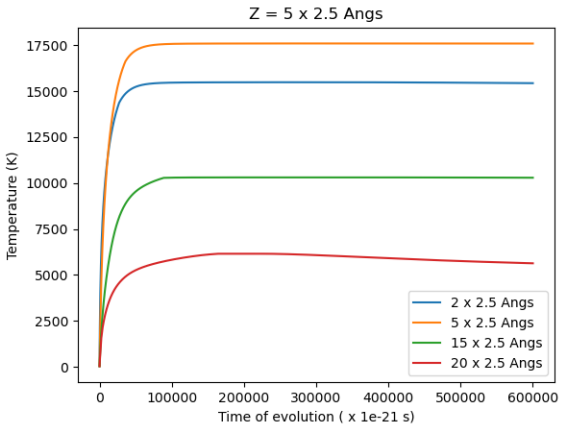


**Figure 6.** Evolution of total temperature with time with varying radius.

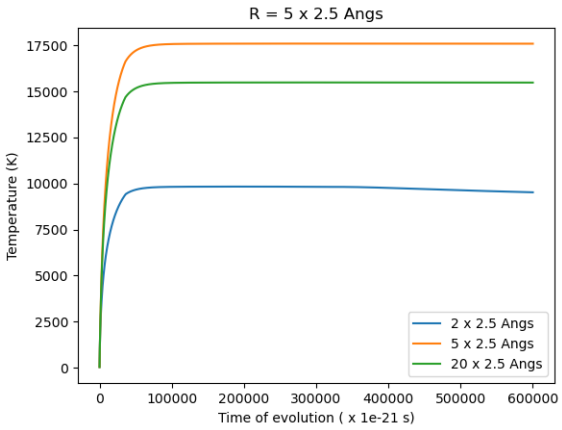


**Figure 7.** Evolution of total temperature with time with varying radius.

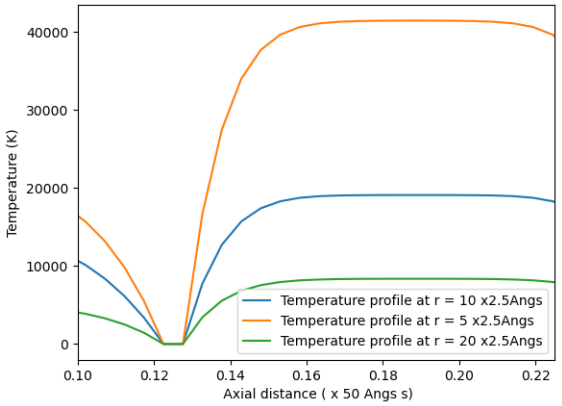


**Figure 8.** Evolution of lattice temperature with axial distance (across contact).

code designed looks at dynamics at very low time scales, the

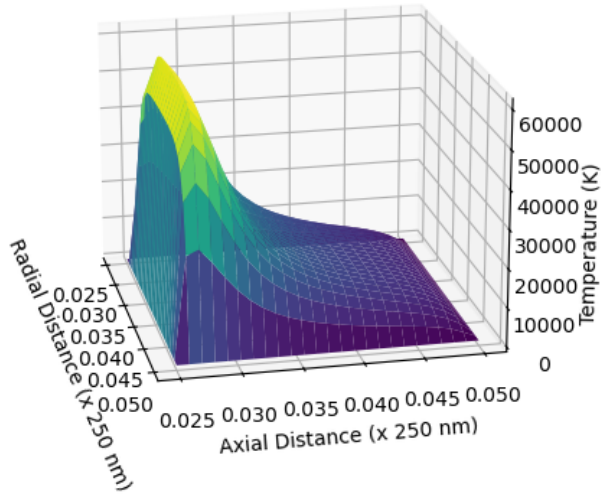


**Figure 9.** Evolution of system 2 lattice temperature with spatial dependence.

system dynamics is restricted by the memory of the computer used. Also, due to the stability condition given by 19, we are restricted to start the system with a O($10^{-21}$) scales, which over time accumulates heavy memory usage. Thus, the number of grids used defines how long we look at the temperatures ($10^{14-15}$s). A high end system (with more RAM) would have helped in understanding the dynamics at longer time scales. Also, we shall see higher temperatures at larger time scales, but is limited by the boundary conditions used. To understand the dynamics, we have assumed here that the system goes to initial temperatues near the the boundary, in reality it may not be the actual case and we will see temperature spikes near the boundaries too. Also, the bilayer system might see a heat backflow since the temperature across the Ni sample is very high compared to the copper sample. The properties of the material affect the temperature gain starkly.

The temporal evolution of temperatures at different radii and axial distances reveals a crossover time, where regions farther from the origin experience higher temperatures than closer regions. This is due to the backflow of heat from these high-temperature regions and the passage of the ion beam through the medium, which raises the temperatures.
The main issue in the calculations were the bottlenecking of the system due to high memory usage. The codes take 4-5 hours for monolayer systems to run, while the codes for bi-layer systems take more. Hence, it was decided to reduce the time scale for bilayer system since the code was bottlenecked by the memory (8 GB).

We also have ignored the effects of heating such as phase transitions as these add extra comlicacy to the system that includes fluid dynamical equations that would be tough to take into account. It is assumed that the heating does not cause melting of the material. Neverthless, the heating can be used to cause irradiation defects in the metal layers.

It is vital to understand that the thermal spike model has limitations. For example, it implies that energy deposition occurs instantaneously and locally, which may not always be the case. It also fails to account for some quantum mechanical effects, which can be crucial at high energy densities.

To summarise, while the thermal spike model provides useful insights into the behaviour of materials under ion irradiation, more study is needed to enhance the model and better comprehend the intricate interplay of numerous physical processes at these high circumstances.

Overall, we found the temperature rise in the material (Cu monolayer and Cu - Ni bilayers) as functions of irradiance, spatial coordinates, densities and time variation. This provides a basic outline for experimental irradiations since the control over the temperature based on irradiance and other properties can be done. Further, these can be used to study phase transitive damage, given by eq 7. These damages are used to produce many interesting properties in multilayered systems, such as quantum dots, nano fabrications, lithography etc. It is important to note that the stopping powers have an error of 10% from precise values as reported by Zhang et.al [15]. Neverthless, the thermal spike model is a strong tool, which we utilised to the study the temperature dynamics of an irradiated system and can be used as a base to experimentally verify the results.

## References


[1] P.I Gaiduk, F.F Komarov, and W Wesch. Damage evolution in crystalline inp during irradiation with swift xe ions. *Nuclear Instruments and Methods in Physics Research Section B: Beam Interactions with Materials and Atoms*, 164-165:377–383, 4 2000.

[2] P.I. Gaiduk, A.Nylandsted Larsen, and J.Lundsgaard Hansen. Strain-relaxed sige/si heteroepitaxial structures of low threading-dislocation density. *Thin Solid Films*, 367:120–125, 5 2000.

[3] Radiation damage. In Jaroslav Koutsky and Jan Kocik, editors, *Radiation Damage of Structural Materials*, volume 79 of *Materials Science Monographs*, pages 22–65. Elsevier, 1994.

[4] R.L.Fleischer, P.B.Price, and R.M. Walker. Ion explosion spike mechanism for formation of charged-particle tracks in solids. *Journal of Applied Physics*, 36:3645–3652, 11 1965.

[5] James F.Ziegler, M.D.Ziegler, and J.P.Biersack. Srim the stopping and range of ions in matter (2010). *Nuclear Instruments and Methods in Physics Research Section B: Beam Interactions with Materials and Atoms*, 268:1818–1823, 6 2010.

[6] I. V. Amirkhanov, A. Yu Didyk, E. V. Zemlyanaya, I. V. Puzynin, T. P. Puzynina, N. R. Sarkar, I. Sarkhadov, V. K. Semina, Z. A. Sharipov, and A. Hofman. Numerical investigation of temperature effects in materials irradiated by high-energy heavy ions in the framework of heat conduction equation for electrons and lattice. *Physics of Particles and Nuclei Letters*, 3:37–45, 1 2006.

[7] E.Balanzat and S.Bouffard. Basic phenomena of the particle-matter interaction. *Solid State Phenomena*, 30-31:7–74, 1 1992.

[8] Marcel Toulemonde, William J. Weber, Guosheng Li, Vaithiyalingam Shutthanandan, Patrick Kluth, Tengfei Yang, Yuguang Wang, and Yanwen Zhang. Synergy of nuclear and electronic energy losses in ion-irradiation processes: The case of vitreous silicon dioxide. *Physical Review B*, 83:054106, 2 2011.

[9] Z G Wangts, Ch Dufourtt, E Paumiertt, and M Toulemoude. The se sensitivity of metals under swift-heavy-ion irradiation: a transient thermal process, 1994.

[10] Frank Elson, Debarchan Das, Gediminas Simutis, Ola Kenji Forslund, Ugne Miniotaite, Rasmus Palm, Yasmine Sassa, Jonas Weissenrieder, and Martin Mnsson. Trim simulations tool for ? +stopping fraction in hydrostatic pressure cells. volume 2462. Institute of Physics, 2023.

[11] A. Chettah, H. Kucal, Z. G. Wang, M. Kac, A. Meftah, and M. Toulemonde. Behavior of crystalline silicon under huge electronic excitations: A transient thermal spike description. *Nuclear Instruments and Methods in Physics Research, Section B: Beam Interactions with Materials and Atoms*, 267:2719–2724, 8 2009.

[12] D. P. Datta, A. Chettah, V. Siva, D. Kanjilal, and P. K. Sahoo. Dewetting induced au-ge composite nanodot evolution in sio 2. *Applied Surface Science*, 428:676–683, 1 2018.

[13] K Yasui. Thermal spike model of defect production by electron excitation in cu, 1994.

[14] M. Toulemonde, E. Paumier, and C. Dufour. Thermal spike model in the electronic stopping power regime. *Radiation Effects and Defects in Solids*, 126:201–206, 3 1993.

[15] Yanwen Zhang, In Tae Bae, Kai Sun, Chongmin Wang, Manabu Ishimaru, Zihua Zhu, Weilin Jiang, and William J. Weber. Damage profile and ion distribution of slow heavy ions in compounds. *Journal of Applied Physics*, 105, 2009.